Journal of Hydroscience and Hydraulic Engineering
Vol. 9, No. 2, January, 1992, 27-35

THE UNSTEADY FLOW STRUCTURE BEHIND A BACKWARD-FACING STEP IN AN OPEN CHANNEL

By

Kiyosi KAWANISI

Department of Civil Engineering, Hiroshima University
Higashi Hiroshima, 724, JAPAN

and

Shōitirō YOKOSI

Department of Civil Engineering, Hiroshima University
Higashi Hiroshima, 724, JAPAN

SYNOPSIS

Instantaneous two-dimensional velocity fields behind a backward-facing step in an open channel are investigated using flow visualization and digital image processing. Measurements extend to a distance of about 35 step-heights downstream of the step, and include parts of the recirculating flow region. The Reynolds number based on step height is 1.6×10^4. Instantaneous spatial distributions of velocity, pressure and vorticity are presented and discussed in three longitudinal sections and two horizontal sections. Space-time distribution of the longitudinal velocity close to the channel bed and the temporal variation of spanwise vorticity are estimated in order to clarify the low-frequency unsteadiness in the separation bubble. The low-frequency unsteadiness seems to be dependent on the strength of spanwise vorticity in the reattachment zone. It is observed that the high Reynolds shear stresses, which are produced by the large-scale eddies, intermittently appear at downstream locations of the step. It appears that the separated shear layer reaches a fully three-dimensional state (hairpin-like) soon after separation, being grouped along the spanwise direction.

INTRODUCTION

The turbulent, separating and reattaching flows in fluid equipments such as diffusers have been studied by many researchers over the years because of its practical importance. On the other hand, turbulent flow with separation and reattachment over an alluvial river bed has been studied in connection with the transportation of sediment, the formation of sand waves and so on (see e.g. Matthes (9), Jackson (4), Ueno & Utami (10)).

The flow over a backward-facing step has been a classic example of the phenomena of separation, recirculation, reattachment, and subsequent relaxation of the shear layer, and it has been studied extensively for several years; nevertheless, it is still far from being well understood.

It is necessary to successively measure an instantaneous velocity field to explicate the structure of turbulent flow with separation and reattachment. However, it is scarcely possible to measure an instantaneous velocity field with high resolution in space using velocimeters; therefore, few examples of successive measuring of instantaneous velocity fields behind a backward-facing step have been shown in the previous works.

It is the objective of this paper to investigate flow characteristics in the separated shear layer, the reattachment zone, and the redeveloping boundary

layer downstream of reattachment. This paper presents successive measurements of instantaneous velocity fields, which were investigated using flow visualization and digital image processing, behind a backward-facing step.

EXPERIMENTS

The flow-visualization experiments were conducted on the bed of an open channel which was 30 m long and 0.8 m wide. The bed and side walls of the open channel are made of smooth steel and glass except at the test sections which are only made of glass. A backward-facing step, which was made of acrylic plates, was placed 15.2 m from the upstream edge of the channel. The step height, H_S , was 4.0 cm.

The coordinates and the positions of three vertical longitudinal test sections are shown in Fig. 1. All measurements were performed at a water discharge of 25 l/s and channel slope of 1/700. The flow depth, H_0 , and maximum local mean velocity, U_0 , at the step were 0.115 m, 0.4 m/s, respectively, and the expansion ratio $H_0/(H_0 - H_S)$ was 1.53.

The three vertical longitudinal sections and two horizontal sections were illuminated separately by a light sheet. The polystyrene particles with a mean diameter of 0.5 mm were used as tracers, which were firstly mixed with the water of a tank and supplied to the flow water at the position of 4 m upstream of the step.

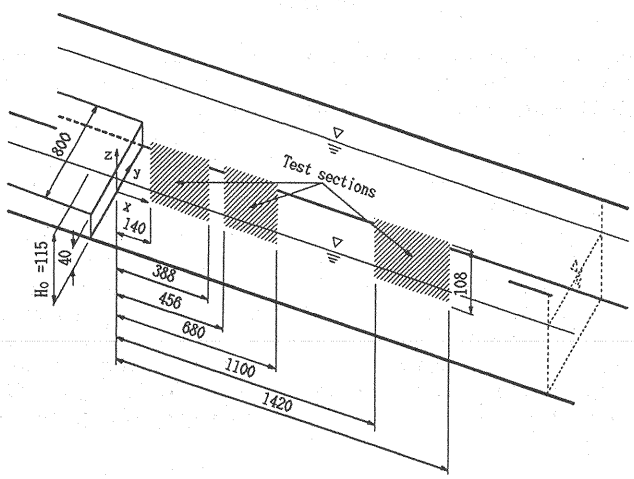

Fig. 1 Backward-facing step, coordinates system and longitudinal test sections, Dimensions in mm

A 35 mm camera with motor drive, allowing a maximum rate of 3.3 frames per second was used. The photographic time interval was 317 ms, in the case of our usual exposure time of 31.4 ms. The negative films of 400 ASA were overdeveloped to 3200 ASA. Positive images were all printed on 17 × 12 cm photographic paper of high contrast. Digitization of the traces on photographic paper with a reduced scale 1/2 or so was done by an image scanner which has the resolving power of 80 pixels/cm. After conducting expansion and contraction processing on the binary images, micro connected components were eliminated, so that the binary images were smoothed and noisy components removed. Then the mean location of the particle paths and the two components of the corresponding velocity vectors were computed and put into the external memory of a personal computer. The direction of velocity vectors in the recirculating region was determined manually from the pattern of particle-tracing photograph (Kawanisi & Yokosi (5)). A square grid pattern was imagined as covering the entire photographic field with a view to numerical calculations, and at each of the mesh points velocity vector was interpolated from neighboring velocity vectors which are randomly distributed (Kobayashi et al. (8)). The mesh intervals corresponded to

1/5 of H_S.

RESULTS AND DISCUSSION

Velocity and pressure fields associated with large-scale vortices

The results of the processing traces on a photograph of longitudinal section are shown in Fig. 2, which include instantaneous velocity and fluctuating velocity vectors in a longitudinal section at the elapsed time $tU_0/H_S = 9.5$. The velocity fluctuations are obtained by subtracting the mean values which are determined from 37 consecutive frames. We observe in Fig. 2 the large-scale vortices, which may be generated in the separating shear layer, convectively move downstream.

Fig. 2(b) shows the large-scale vortices of clockwise rotation which corresponds to the large structures in Fig. 2(a). This figure also shows a rotating system in the counterclockwise sense exists in between two the large-scale eddies observed in Fig. 2(a). The convective velocity of the large-scale vortices determined from the consecutive fluctuating velocity fields, is $0.4U_0$–$0.7U_0$, which is consistent with the previously published values (Kiya & Sasaki (6)) in the case of separation at the leading edge of a blunt flat plate. One can observe strong outflows from the wall toward the main stream on the upstream side of the vortices in Fig. 2.

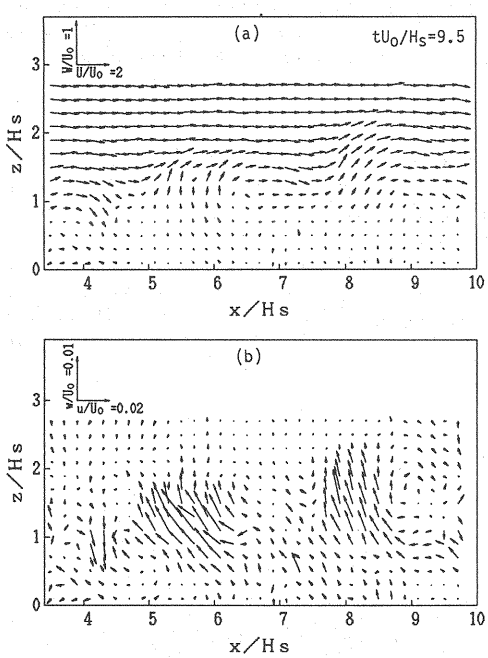

Fig. 2 Instantaneous distribution of velocity and fluctuating velocity vectors in a longitudinal section

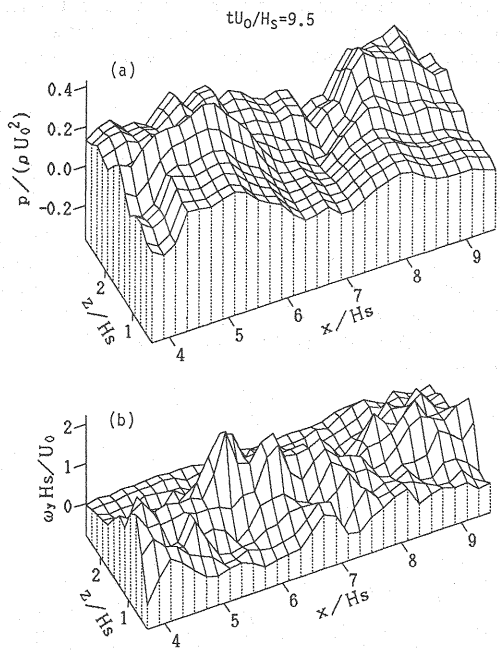

Fig. 3 Instantaneous distribution of pressure and spanwise vorticity in a longitudinal section

Fig. 3(a) shows an instantaneous pressure distribution in the same longitudinal section and elapsed time as Fig. 2. The instantaneous distribution of pressure is obtained from a series of numerical integrations of the unsteady two-dimensional Navier-Stokes equation without gravity term; that is

$$\frac{\partial U}{\partial t} + U\frac{\partial U}{\partial x} + W\frac{\partial U}{\partial z} = -\frac{1}{\rho}\frac{\partial p}{\partial x} + \nu\left(\frac{\partial^2 U}{\partial x^2} + \frac{\partial^2 U}{\partial z^2}\right)$$

$$\frac{\partial W}{\partial t} + U\frac{\partial W}{\partial x} + W\frac{\partial W}{\partial z} = -\frac{1}{\rho}\frac{\partial p}{\partial z} + \nu\left(\frac{\partial^2 W}{\partial x^2} + \frac{\partial^2 W}{\partial z^2}\right) \qquad (1)$$

In these equations the pressure gradients $\partial p/\partial x$ and $\partial p/\partial z$ are computed first from the measured values of other terms, all the derivatives of U and W evaluated by using the cubic spline function. Then the integration of these pressure gradients are iterated from the starting point situated in the center of the grid area. Assume, the initial value of the pressure at the center point is 0. The pressure gradients are integrated on two routes and arithmetically averaged. It can be seen that the instantaneous pressure fluctuations are produced by the large-scale eddies in Fig. 2(b). The pressure fluctuation attains a valley of sufficient depth under a large system of rotating flow in the clockwise sense (Fig. 2b). On the other hand, the pressure fluctuation attains a peak under a rotating system in the counterclockwise sense, in other words, between large eddies observed in Fig. 2(a). These results are consistent with the conditionally averaged velocity fluctuations and surface pressure fluctuations reported by Kiya and Sasaki (6). The pressure above a large-scale eddy is high unlike that under the eddy.

Fig. 3(b) shows the spanwise component $\omega_y = \partial u/\partial z - \partial w/\partial x$ of the instantaneous vorticity in the same longitudinal section and elapsed time of Fig. 2 and Fig. 3(a). The vorticity is estimated from the velocity gradients at the meshpoints, with the aid of finite-difference approximation of the definitive formula expressed in two-dimensional form. Clearly, the concentrations of spanwise vorticity can be seen near the center of the rotating system in the clockwise sense. On the other hand, the strong concentrations of the vorticity are not observed near the center of the rotating system in the counterclockwise sense; therefore, it is not an actual vortex. Thus, we interpret this rotating system as being induced by the large-scale vortices as Kiya & Sasaki (6) have reported.

Instantaneous distribution of the Reynolds shear stress

The time-space distribution of the instantaneous Reynolds shear stress at the time-mean reattachment point $(x/H_S = 8.1)$, and at point $x/H_S = 14.0$ can be observed in Fig. 4(a),(b). It is known that the high shear stresses intermittently appear and may be produced by the large-scale eddies. These results suggest that the Reynolds shear stress is mainly contributed by the large-scale eddies and the estimation of the Reynolds stress behind a backward-facing step needs average instantaneous stress over a long time. The peaks of the instantaneous Reynolds stress at $x/H_S = 14.0$ compared with $x/H_S = 8.1$ are at an upper location.

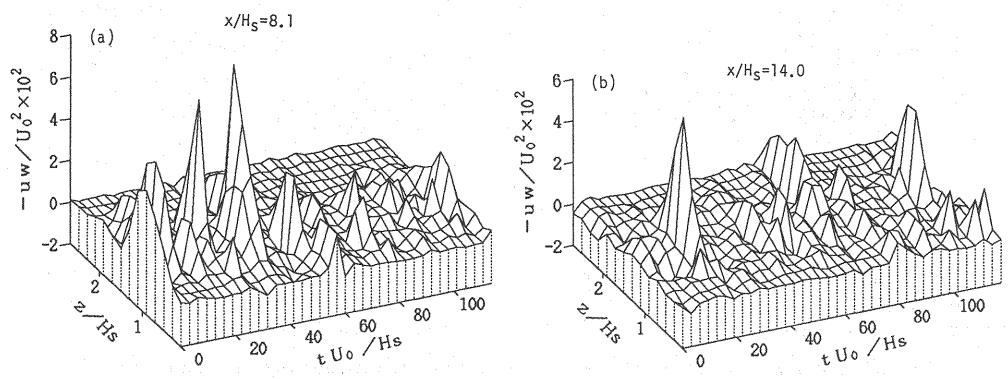

Fig. 4 Space-time distributions of the instantaneous Reynolds shear stress at stream-wise sections $x/H_S = 8.1$ and 14.0

Low frequency unsteadiness

In this section properties of low frequency unsteadiness behind a backward-facing step will be presented and discussed. It has been reported in previous studies (Eaton & Johnston (2), Cherry et al. (1), Kiya & Sasaki (7)) that the

unsteady flow in the reattaching zone is mainly governed by two agents: the motion of the large-scale vortices and the low-frequency unsteadiness in connection with a weak flapping of the separated shear layer. Cherry et al. (1), Kiya & Sasaki (7) investigated the low-frequency unsteadiness in the surface pressure signal, which is measured at a short distance downstream of the separation line formed by the two-dimensional rectangular leading-edge geometry. Because the low-frequency unsteadiness is observed everywhere in the separation bubble, the scale of low-frequency disturbance is large.

Fig. 5(a) shows a longitudinal velocity map as a function of x and t at $y/H_S = 0.0$ and $z/H_S = 0.1$. To study properties of the low-frequency unsteadiness, a moving average with a time-mean length 0.634 s is done on the instantaneous velocity. Distance between iso-velocity lines is $U/U_0 = 0.05$. The solid and dashed lines correspond to the positive and negative values, respectively. The thick solid isoline corresponds to the temporal variation of the instantaneous reattaching point. We interpret a position, where the velocity at the height of $z/H_S = 0.1$ in the reattaching zone attains zero, as an instantaneous reattachment position. A low-frequency growing and shrinking process of the separation bubble is observed in Fig. 5(a). The shrinking of the separation bubble is much swifter than it's growing, compatible to the result of Kiya & Sasaki (7). The reason for the large-scale, low-frequency unsteadiness that occurs in this case is not fully understood. Gai & Sharma (3) have reported that the reattachment length is decreased by the acceleration of three-dimensional state of the separated shear layer. The results suggest that the large-scale, low-frequency variation of the separation bubble has been produced by the change of three dimensional state in the initial recirculation region.

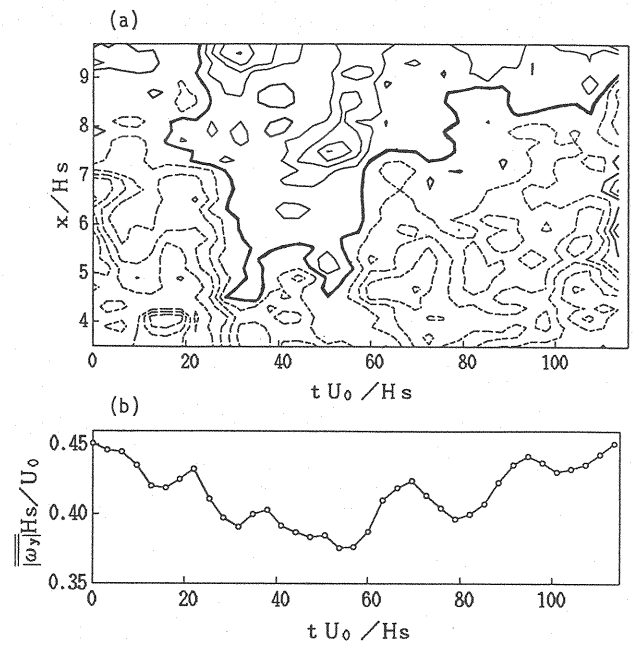

Fig. 5 (a) Space-time distribution of isolines of instantaneous longitudinal velocity close to the channel bed; (b) Variation of spanwise vorticity averaged over the longitudinal section

Fig. 5(b) shows the variation of spanwise vorticity, which is averaged over the longitudinal section after converting to the absolute value. A time-mean length of a moving average is equal to one used in the calculation to get Fig. 5(a). The low-frequency unsteadiness in the bubble seems to be dependent on the phase of the strength of the spanwise vorticity in Fig. 5(b). The bubble is growing as the spanwise vorticity becomes larger. On the contrary, when the

vorticity becomes smaller, the bubble is shrinking.

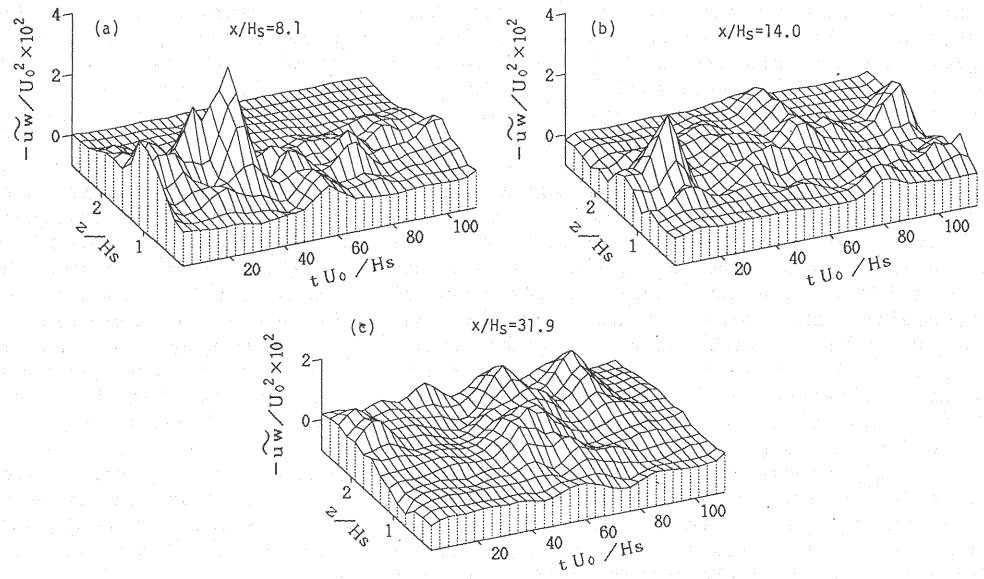

Fig. 6 Space-time distributions of the moving time averaged Reynolds shear stress at stream-wise sections $x/H_S = 8.1, 14.0$ and 31.9

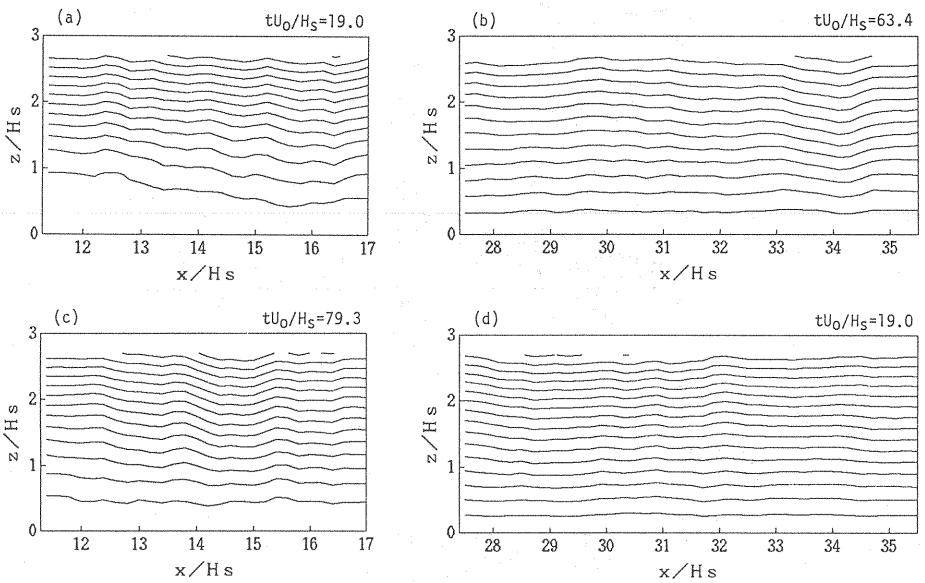

Fig. 7 Distributions of moving time averaged streamline in two longitudinal section

It is considered that the large-scale, low-frequency growing and shrinking process of the separation bubble largely influences the flow behind a backward-facing step. Fig. 6 shows the variations of the Reynolds shear stress profile on which a moving average with a time-mean length equal to one in the calculation to get Fig. 5 is done. The space-time distributions of the Reynolds stress at three downstream locations are shown in Fig. 6 (a), (b) ,(c) at $x/H_S = 8.1, 14.0$ and 31.9, respectively. It seems that the time interval of the occurrences of the high Reynolds stress is large in association with the low-frequency un-

steadiness of the separation bubble.

Fig. 7 shows the streamline distributions on which a moving average with a time-mean length equal to one in the calculation to get Figs. 5 and 6 is done. The streamline distributions in the consecutive two downstream longitudinal sections are shown. The contour maps in Fig. 7(a), (b) and (c), (d) show the streamline distributions when the Reynolds stress in Fig. 6 is high and low, respectively. The distance between isolines is $\psi/U_0H_S = 0.1$. The low-frequency variation is found in the streamline distributions and the number of isolines are larger in Fig. 7(c),(d) than (a), (b). Since the convective velocity of the large-scale eddy, which generates the high Reynolds stress, is smaller than the mean velocity, the lower velocity corresponds to the higher Reynolds stress.

Properties of flow fields in horizontal section

Fig. 8 shows the instantaneous distributions of the longitudinal velocity and vertical component $\omega_z = \partial v/\partial x - \partial u/\partial y$ of vorticity in the two horizontal sections ($x = 1.6$–16.0 cm, $y = -11.6$–11.6 cm, $z = 5.0$ cm and $x = 52.0$–66.4 cm, $y = -11.6$–11.6 cm, $z = 7.0$ cm). It appears that the shear layer reaches a fully three-dimensional state soon after separation. The low speed regions exist between positive and negative peaks of vorticity in the spanwise direction. This result suggests that hairpin-like vortices exist in the flow behind the backward-facing step. The spanwise distance between the low speed regions in Fig. 8(a) is roughly 1–$2H_S$ (0.5–$1.0x_R$; x_R = time-mean reattachment length). This value is consistent with that reported by Kiya & Sasaki (6). On the other hand, the spanwise distance between the low speed regions in Fig. 8(b) is roughly 3–$4H_S$, and is larger than a short distance downstream of the separation line in Fig. 8(a). The low speed regions of Fig. 8(b) extend in the direction of x.

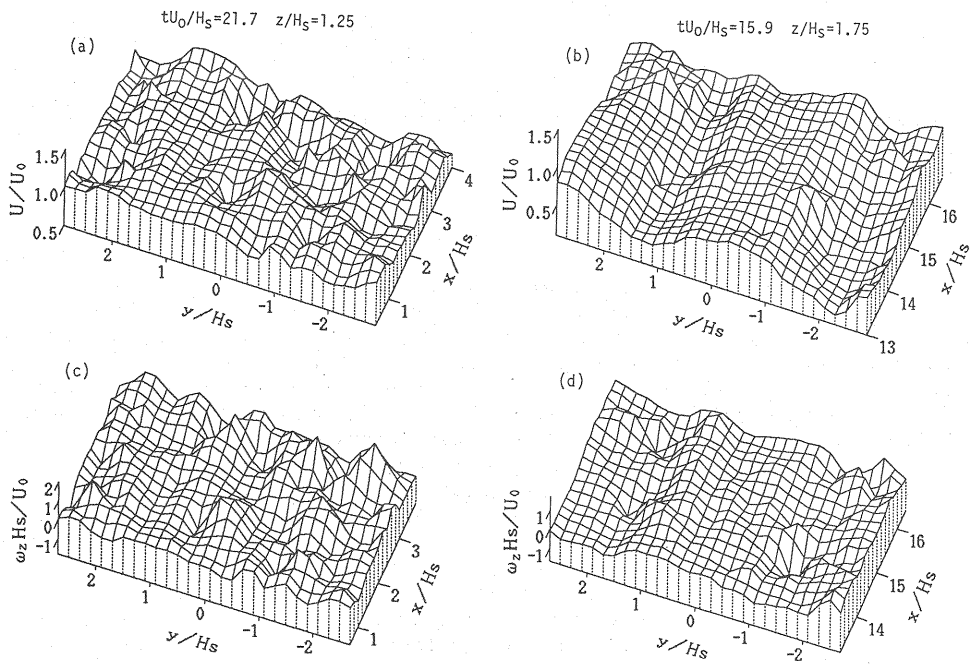

Fig. 8 Instantaneous distributions of longitudinal velocity and vertical vorticity in horizontal sections

Fig. 9 shows instantaneous pressure distributions in the same sections as Fig. 8. The instantaneous distributions of pressure are estimated by the same way as Fig. 3(a). One of the features concerning the pressure distributions is the series of crests and troughs that are oriented approximately parallel to the span, though they are often skewed rather than being perfectly two-dimensional.

It seems that the negative and positive peaks of vorticity in Fig. 8(c), (d) exist near the crest. Based on the series of crests in Fig. 9, it is considered that hairpin-like vortices are grouped along the spanwise direction. This has been already indicated by Kiya & Sasaki (6).

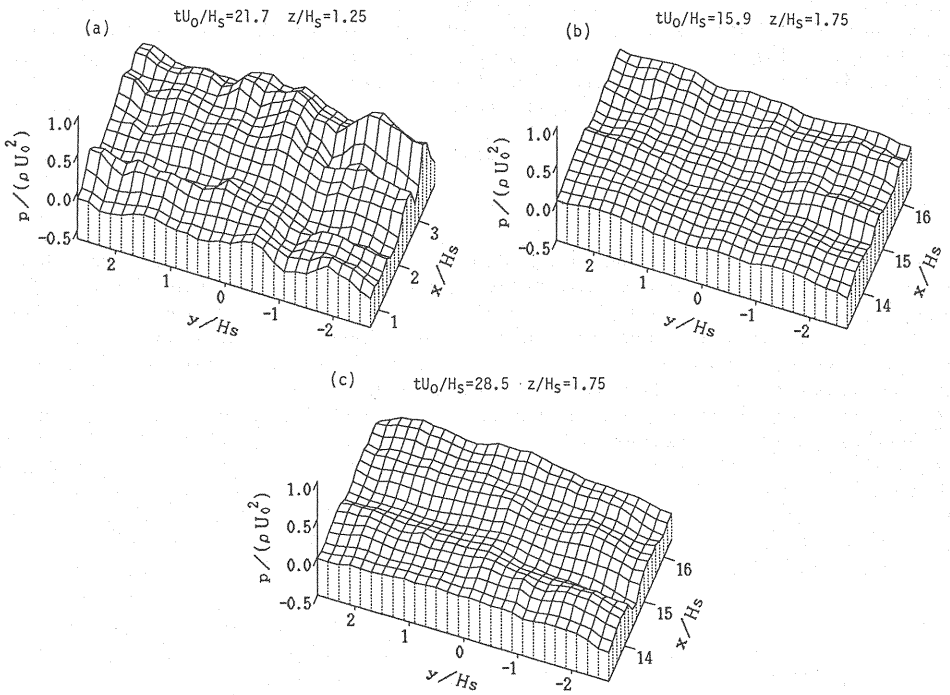

Fig. 9 Instantaneous distributions of pressure in horizontal section

CONCLUSIONS

The unsteady properties of flow behind a backward-facing step in an open channel have been investigated from flow visualization experiments. The main conclusions of this paper can be summarized as follows.

1. The convective velocity of the large-scale vortices in the reattachment zone is 0.4–$0.7U_0$, which is consistent with previous reported values in the case of separation at the leading edge of a blunt flat plate.

2. The surface pressure fluctuations are related with the large-scale vortices shedding from the separation bubble. The surface pressure is low under the large-scale eddies, and it is high in between two large-scale eddies.

3. It is observed that the high instantaneous Reynolds shear stresses are intermittently generated at downstream locations of the step. The high Reynolds stresses are produced by the large-scale eddies. The results suggest that the Reynolds shear stress is mainly contributed by the large-scale eddies.

4. The low-frequency variation of the separation bubble seems to be dependent on the phase of the strength of the spanwise vorticity. The bubble is growing when the spanwise vorticity becomes larger. On the contrary, when the vorticity becomes smaller, the bubble is shrinking.

5. The low speed regions in horizontal sections exist between positive and negative peaks of a vertical vorticity component in the spanwise direction. The spanwise distance between the low speed regions is roughly 1–$2H_S$ at a short distance downstream of the separation line. By observing the flow to downstream, the spanwise distance grows larger (roughly 3–$4H_S$).

6. The features of the pressure distributions in horizontal sections are the series of crests and troughs that are oriented approximately parallel to the span, though they are often skewed rather than being perfectly two-dimensional.

It seems that the negative and positive peaks of vorticity in the sections exist near the crest.

REFERENCES

1. Cherry, N.J., R. Hillier and M.E.M. Latour : Unsteady measurements in a separated and reattaching flow, J. Fluid Mech., Vol.144, pp.13-46, 1984.
2. Eaton, J.K. and J.P. Johnston : Turbulent flow reattachment: An experimental study of the flow and structure behind a backward-facing step, Dept. of Mechanical Engineering, Stanford Univ., Rept. MD-39, 1980.
3. Gai, S.L. and S.D. Sharma : Subsonic turbulent flow over a rearward facing segmented step, Phys. Fluids, Vol.27, No.3, pp.544-546, 1984.
4. Jackson, R.G. : Sedimentological and fluid-dynamic implications of the turbulent bursting phenomenon in geophysical flows, J. Fluid Mech., Vol.77, pp.531-560, 1976.
5. Kawanisi, K. and S. Yokosi : Coherent motion of a turbulent flow behind a backward-facing step in open channel, Proc. 33th Japanese Conf. Hydraul., 1989.
6. Kiya, M. and K. Sasaki : Structure of a turbulent separation bubble., J. Fluid Mech., Vol.137, pp.83-113, 1983.
7. Kiya, M. and K. Sasaki : Structure of large-scale vortices and unsteady reverse flow in the reattaching zone of a turbulent separation bubble, J. Fluid Mech., Vol.154, pp.463-491, 1985.
8. Kobayashi, T., H. Matsumoto and T. Saga : Visual simulation of turbulent flow in two-dimensional channel with steps, J. Flow Visual. Soc. Japan, Vol.5, No.18, 1985.
9. Matthes, G.H. : Macroturbulence in natural stream flow, Trans., A.G.U., Vol.28, No.2, pp.255-265, 1947.
10. Ueno,T. and T. Utami : Experimental study on the development of ripples and dunes, Proc. JSCE, No.318, pp.75-84, 1982.

APPENDIX - NOTATION

The following symbols are used in this paper:

H_0	= flow depth at step;
H_S	= step height;
p	= pressure;
t	= elapsed time;
u,v,w	= fluctuating velocity components in x, y and z directions, respectively;
U,V,W	= velocity components in x, y and z directions, respectively;
U_0	= maximum local mean velocity at step;
x,y,z	= coordinates as defined in Fig. 1;
x_R	= reattachment length;
ρ	= density of water;
ψ	= stream function; and
ω_y,ω_z	= vorticity components in y and z directions, respectively.

Superscripts

$\sim$	= moving time averaged value; and
$=$	= averaged value over longitudinal section.

(Received July 30, 1990; revised February 7, 1991)